1521-009X/50/6/734–740$35.00
DRUG METABOLISM AND DISPOSITION

dx.doi.org/10.1124/dmd.122.000868
Drug Metab Dispos 50:734–740, June 2022

Characterizing and Quantifying Extrahepatic Metabolism of (−)-Δ^9-Tetrahydrocannabinol (THC) and Its Psychoactive Metabolite, (±)-11-Hydroxy-Δ^9-THC (11-OH-THC) [S]

Aditya R. Kumar, Gabriela I. Patilea-Vrana, Olena Anoshchenko, and Jashvant D. Unadkat

Department of Pharmaceutics, University of Washington, Seattle, Washington

Received February 10, 2022; accepted March 31, 2022

ABSTRACT

(−)-Δ^9-Tetrahydrocannabinol (THC) is the psychoactive constituent of cannabis, a drug recreationally consumed orally or by inhalation. Physiologically based pharmacokinetic (PBPK) modeling can be used to predict systemic and tissue exposure to THC and its psychoactive metabolite, (±)-11-hydroxy-Δ^9-THC (11-OH-THC). To populate a THC/11-OH-THC PBPK model, we previously characterized the depletion clearance of THC (by CYP2C9) and 11-OH-THC (by UDP-glucuronosyltransferase (UGT), CYP3A, and CYP2C9) in adult human liver microsomes. Here we focused on quantifying extrahepatic depletion clearance of THC/11-OH-THC, important after oral (intestine) and inhalational (lung) consumption of THC as well as prenatal THC use (placenta and fetal liver). THC (500 nM) was metabolized in adult human intestinal microsomes (n = 3–5) by CYP2C9 [V_{max}: 1.1 ± 0.38 nmol/min/mg; Michaelis-Menten constant (K_m): 70 nM; intrinsic clearance (CL_{int}): 15 ± 5.4 ml/min/mg; fraction metabolized (fm): 0.89 ± 0.31 at concentration ≪ 70 nM] and CYP3A (CL_{int}: 2.0 ± 0.86 ml/min/mg; fm: 0.11 ± 0.050). 11-OH-THC (50 nM) was metabolized by CYP3A (CL_{int}: 0.26 ± 0.058 ml/min/mg; fm: 0.51 ± 0.11) and UGT2B7 (CL_{int}: 0.13 ± 0.027 ml/min/mg; fm: 0.25 ± 0.053). THC at 500 nM (CL_{int}: 4.7 ± 0.22 ml/min/mg) and 11-OH-THC at 50 nM (CL_{int}: 2.4 ± 0.13 ml/min/mg) were predominately (fm: 0.99 and 0.80, respectively) metabolized by CYP3A in human fetal liver microsomes (n = 3). However, we did not observe significant depletion of THC/11-OH-THC in adult lung, first trimester, second trimester, or term placentae microsomes. Using PBPK modeling and simulation, these data could be used in the future to predict systemic and tissue THC/11-OH-THC exposure in healthy and special populations.

SIGNIFICANCE STATEMENT

This is the first characterization and quantification of (−)-Δ^9-tetrahydrocannabinol (THC) and (±)-11-hydroxy-Δ^9-THC (11-OH-THC) depletion clearance by cytochrome P450 and UDP-glucuronosyltransferase enzymes in extrahepatic human tissues: intestine, fetal liver, lung, and placenta. These data can be used to predict, through physiologically based pharmacokinetic modeling and simulation, systemic and tissue THC/11-OH-THC exposure after inhalational and oral THC use in both healthy and special populations (e.g., pregnant women).

Introduction

Cannabis is the most frequently used recreational drug in the United States. It is primarily consumed orally or by inhalation, and with increased legalization, its use has also increased. Currently, 17.9% of the United States adult population (age 12 or older) uses cannabis (SAMHSA, 2021). Due to psychoactive effects of (-)-Δ^9-tetrahydrocannabinol (THC) (Amin and Ali, 2019) and its active metabolite, (±)-11-hydroxy-Δ^9-THC (11-OH-THC), changes in exposure to these cannabinoids could cause possible negative outcomes [e.g., anxiety and panic attacks (Grotenhermen, 2003)] when their clearance (CL) is altered by drug-drug interactions (DDIs), genetic polymorphisms, or physiologic changes (e.g., hepatic impairment).

Physiologically based pharmacokinetic (PBPK) modeling is a useful tool to mechanistically predict human THC and 11-OH-THC exposure in silico. PBPK modeling integrates physiologic processes, drug specific physicochemical properties, and in vitro metabolism and transport parameters to predict a drug's disposition in the body. In addition to using a healthy adult PBPK model to estimate THC/11-OH-THC exposure in different genetic populations or in the presence of DDIs, such a model can be extended to predict the disposition of these cannabinoids in special populations that are difficult to study, such as people with hepatic impairment or pregnant women. A pregnancy PBPK model

This work was supported by National Institutes of Health National Institute on Drug Abuse [Grant P01 DA032507] and by National Institutes of Health National Institute of General Medical Sciences [Grant T32 GM007750] (to A.R.K.).

No author has an actual or perceived conflict of interest with the contents of this article.

These data were previously presented in part as follows: Kumar AR (2021) Characterizing and quantifying extrahepatic metabolism of (-)-Δ^9-tetrahydrocannabinol (THC) and its psychoactive metabolite, 11-OH-THC. *24th North American International Society for the Study of Xenobiotics (ISSX) Virtual Meeting;* 2021 Sept 13–17; held virtually. International Society for the Study of Xenobiotics, Washington, DC.

dx.doi.org/10.1124/dmd.122.000868.

[S] This article has supplemental material available at dmd.aspetjournals.org.

ABBREVIATIONS: ANF, alpha-naphthoflavone; AUC, area under the curve; AZA, azamulin; BSA, bovine serum albumin; CL, clearance; CL_{FH}, fetal liver clearance; CL_{GI}, intestinal clearance; CL_{int}, intrinsic clearance; 11-COOH-THC, (±)-11-nor-9-carboxy-Δ^9-THC; DDI, drug-drug interaction; 7-ER, 7-ethoxyresorufin; F_g, fraction that escapes the gut; FLZ, fluconazole; fm, fraction metabolized; FMO, flavin-containing monooxygenase; G6P/G6PDH, D-glucose 6 phosphate/glucose-6-phosphate dehydrogenase; HFLM, human fetal liver microsome; HIM, human intestinal microsome; HLuM, human lung microsome; HPM, human placental microsome; ITZ, itraconazole; K_m, Michaelis-Menten constant; LB, low-binding; LC, liquid chromatography; LC-MS/MS, liquid chromatography-tandem mass spectrometry; MDZ, midazolam; NFA, niflumic acid; 1-OH-MDZ, 1-hydroxymidazolam; 11-OH-THC, (±)-11-hydroxy-Δ^9-THC; P450, cytochrome P450; PBPK, physiologically based pharmacokinetic; RES, resorufin; SFZ, sulfaphenazole; T1, trimester 1; T2, trimester 2; THC, (−)-Δ^9-tetrahydrocannabinol; UGT, UDP-glucuronosyltransferase.

could help predict fetal THC/11-OH-THC exposure throughout gestation after maternal cannabis consumption. Such predictions are important due to the potential deleterious effects of cannabis to the fetus/infant (Day et al., 1994; Goldschmidt et al., 2000, 2008, 2012; Paul et al., 2021).

To build a THC PBPK model, we first need to quantify and then populate the model with the intrinsic metabolic and transport clearance (CL_{int}) of THC and 11-OH-THC. Because THC and 11-OH-THC are predominantly cleared from the body by metabolism [and do not appear to be significantly transported (Chen et al., 2021)], here we focused on quantifying the metabolic depletion CL of THC and 11-OH-THC in tissues that could potentially contribute to the overall CL of THC and 11-OH-THC from the body after inhalation or oral cannabis consumption. Because THC is cleared from the body primarily by metabolism (Lucas et al., 2018), we previously characterized and quantified the hepatic depletion CL of THC and 11-OH-THC, in which we found that THC was predominately metabolized by CYP2C9 whereas 11-OH-THC was metabolized by CYP2C9, CYP3A, and UDP-glucuronosyltransferase (UGT) enzymes (Patilea-Vrana and Unadkat, 2019). In addition, through these studies and those with recombinant cytochrome P450 (P450) enzymes, we found that THC could be metabolized by P450 enzymes present in the lung [CYP1A1 (Hukkanen et al., 2001)] and in the intestine [CYP3A4/5, CYP2C9, CYP2C19, CYP2D6, UGTs (Drozdzik et al., 2018)]. Therefore, the tissues of interest here were the intestine and the lung since THC is primarily consumed orally and by inhalation and these organs could lead to both first pass and systemic CL of THC. In addition, to populate our maternal-fetal–PBPK model (Zhang et al., 2017), we also characterized the metabolism of THC and 11-OH-THC in the human placenta and fetal liver. Indeed, our studies with recombinant P450 enzymes showed that THC/11-OH-THC can be metabolized by P450s that are present in the fetal liver [CYP3A7 (Leeder et al., 2005)] or in the placenta [CYP1A1 (Hakkola et al., 1998)].

Materials and Methods

Chemicals and Reagents. THC (1 mg/ml), 11-OH-THC (1 mg/ml), and (±)-11-nor-9-carboxy-Δ^9-THC (11-COOH-THC) (1 mg/ml) DEA-exempt methanol stocks and deuterated internal standards [IS; (-)-Δ^9-THC-D_3, (±)-11-OH-THC-D_3, (±)-11-COOH-THC-D_3] were purchased from Cerilliant (Round Rock, TX). Low-binding (LB) microcentrifuge tubes (made out of chemical-resistant polypropylene) were purchased from Genesee Scientific (San Diego, CA). Bovine serum albumin (BSA) (Fraction V, heat shock treated), sodium phosphate, sucrose, acetonitrile, liquid chromatography-tandem mass spectrometry (LC-MS/MS)-grade formic acid, liquid chromatography (LC) glass inserts, and LC presplit snap caps were purchased from Fisher Scientific (Hampton, NH). Alamethicin, midazolam (MDZ), 1-hydroxymidazolam (1-OH-MDZ), resorufin (RES), and 7-ethoxyresorufin (7-ER) were purchased from Cayman Chemicals (Ann Arbor, MI). UDP-glucuronic acid, ethylenediaminetetraacetic acid (EDTA), β-nicotinamide adenine dinucleotide phosphate (NADP+), D-glucose 6-phosphate (G6P), glucose-6-phosphate dehydrogenase (G6PDH), phenylmethylsulfonyl fluoride, itraconazole (ITZ), sulfaphenazole (SFZ), omeprazole, alpha-naphthoflavone (ANF), quinidine, methimazole, fluconazole (FLZ), and niflumic acid (NFA) were purchased from Sigma-Aldrich (St. Louis, MO). Azamulin (AZA) was purchased from Toronto Research Chemicals (Toronto, ON).

Biologic Materials. Pooled adult, mixed sex human intestinal microsomes (HIMs) (Lot 1610314: $n = 15$, 10 mg/ml), and human lung microsomes (HLuMs) from cigarette smokers (Lot 1910176: $n = 5$, 10 mg/ml; Lot 1310176: $n = 4$, 10 mg/ml) were purchased from Xenotech (Lenexa, KS). HLuMs from cigarette smokers were chosen as smoking induces CYP1A activity (Smith et al., 2001). Human placentae and fetal liver tissues were acquired from the Birth Defects Research Laboratory (Seattle, WA). Human placental microsomes (HPMs) (2 mg/ml) were prepared as described before from trimester 1 (T1), trimester 2 (T2), and term placentate (Anoshchenko et al., 2020), and the demographics are shown in Supplemental Table 1. Human fetal liver microsomes (HFLMs) (18.6 mg/ml) were prepared from six T2 pooled livers (Supplemental Table 2) as follows. Approximately 1 g of tissue was weighed and homogenized in buffer containing 20 mM sucrose, 50 mM potassium phosphate, 10 mM EDTA, and a protease inhibitor (0.2 mM phenylmethylsulfonyl fluoride) with an Omni Bead Ruptor Homogenizer. The homogenate was then centrifuged at 9,000 × g and 4°C for 20 minutes in Optima L-90K Ultracentrifuge (Beckman Coulter, Brea, CA). The resulting S9 fraction was immediately centrifuged at 100,000 × g and 4°C for 1 hour to yield both the cytosolic and microsomal fractions. Microsomal fractions were resuspended in 300 μl of storage buffer (50 mM potassium phosphate, 20 mM sucrose, 10 mM EDTA), and protein content was quantified by a Pierce bicinchoninic acid assay. T2 livers were used as they were available to us in quantity and size needed to prepare microsomes.

Cannabinoid Incubations. HIMs (0.25 and 0.75 mg/ml for THC and 11-OH-THC incubations, respectively), HFLMs (1 mg/ml), HLuMs (1 and 2 mg/ml), and HPMs (0.5 mg/ml) were incubated in LB tubes with either 500 nM THC or 50 nM 11-OH-THC at pharmacologically relevant systemic concentrations (Patilea-Vrana et al., 2019). Incubations were in 0.1 M potassium phosphate buffer (pH 7.4) containing 0.2% BSA to reduce nonspecific binding to plastic and maximize cannabinoid solubility (300 μl final volume). When depletion in the microsomes was observed, to identify the enzymes involved, THC or 11-OH-THC was incubated in the presence and absence of selective enzyme inhibitors: 10 μM SFZ (CYP2C9), 2 μM ITZ (CYP3A), 1 μM quinidine (CYP2D6), 30 μM omeprazole (CYP2C19), 3 μM ANF (CYP1A), 25 μM methimazole [flavin-containing monooxygenase (FMO)], 2.5 mM FLZ (UGT2B), and 2.5 μM NFA (UGT1A9). Although FLZ and NFA are generally not selective for the enzymes listed, for our purposes they were (see reasons provided in the discussion). However, due to presence of CYP3A7 in the HFLMs (vs. CYP3A4/5 in adults) and an increased selectivity for CYP3A7 compared with ITZ, 5 μM AZA was used as the CYP3A-selective inhibitor for the HFLM incubations. To confirm P450 activity in the HFLM, HLuM, and HPM incubations, 1-OH-MDZ formation from MDZ (CYP3A), RES formation from 7-ER (CYP1A), and β-estradiol formation from testosterone (CYP19) were quantified as positive controls, respectively. P450 and FMO incubations were preincubated at 37°C for 10 minutes in a heated shaking block, and P450-mediated depletion of the cannabinoids was initiated with an NADPH regenerating system (1.3 mM NADP+, 3.3 mM G6P, 3.3 mM magnesium chloride, 0.4 unit/ml G6PDH). For UGT-mediated depletions, the microsomes were preincubated with alamethicin (25 μg/ml) for 15 minutes on ice to allow for pore formation and then preincubated as described above (with the addition of 3.3 mM magnesium chloride. Then, the reaction was initiated with 2.5 mM UDP-glucuronic acid. The incubation period (30–60 minutes) for each set of experiments was optimized to achieve significant substrate depletion to estimate the depletion kinetic parameters with confidence. Depletion of the cannabinoids was terminated by adding 100 μl ice-cold acetonitrile containing the internal standards (250 nM THC-D_3, 250 nM 11-OH-THC-D_3, 250 nM 11-COOH-THC-D_3) to a 50 μl aliquot of the reaction mixture in LB tubes and then mixing using a vortex. Samples were centrifuged at 18,000 × g and 4°C for 10 minutes, and 70 μl of the supernatant was stored at −20°C in LC glass inserts until analysis by LC-MS/MS. Three to five independent experiments were conducted, each in duplicate or triplicate.

LC-MS/MS Analysis. Samples (10 μl injection) were analyzed with an ACQUITY ultraperformance liquid chromatography (UPLC) system (Waters Corporation, Milford, MA) coupled to an AB SCIEX Triple Quad 6500 (SCIEX, Framingham, MA). ACQUITY UPLC ethylene bridged hybrid (BEH) C18 column (1.7 μM 2.1 × 50 mm) attached to a BEH C18 5 mm guard column (Waters Corporation, Milford, MA) was used for chromatographic separation with a mobile phase flow rate of 0.3 ml/min. The mobile phase consisted of acetonitrile and water containing 0.1% formic acid as the organic and aqueous phases, respectively. The chromatographic LC-MS/MS conditions used are provided in Supplemental Table 3. Integration of the chromatographic peaks was performed using Analyst v1.6.2 (Framingham, MA). This method was used for all samples other than placental metabolism, for which a previously published method was used (Patilea-Vrana and Unadkat, 2019).

Estimation of THC and 11-OH-THC Depletion Kinetic Parameters. Depletion data were first corrected for any depletion observed in "no NADPH" incubations. Then, for data from each set of experiments, a THC (eq. 1) or 11-OH-THC (eq. 2) depletion model was simultaneously fitted to the time course of depletion in HIMs, in the absence and presence of P450 inhibitors, using nonlinear regression (Phoenix 8.1; Certara, Princeton, NJ). This allowed us to estimate CL via the different P450 pathways. To avoid identifiability issues, the THC CYP2C9 Michaelis-Menten constant (K_m) value was fixed to 70 nM based on our previous estimate of this parameter in human adult liver microsomes obtained under identical incubation conditions (Patilea-Vrana and Unadkat, 2019).

$$\frac{dA_{THC,\ intestinal}}{dt} = -\left(\frac{V_{max,CYP2C9} * C_{THC}}{K_{m,CYP2C9} + C_{THC}} + CL_{CYP3A} * C_{THC}\right) \quad (1)$$

$$\frac{dA_{11-OH-THC,intestinal,CYP}}{dt} = -(CL_{CYP3A} + CL_{Other\ CYP}) * C_{11-OH-THC} \quad (2)$$

$$\frac{dA_{11-OH-THC,intestinal,UGT}}{dt} = -(CL_{UGT2B7} + CL_{Other\ UGT}) * C_{11-OH-THC} \quad (3)$$

For 11-OH-THC, eq. 2 was fitted to the P450-mediated depletion data and eq. 3 was fitted to the UGT-mediated depletion data. In the above models, CL via CYP2C9, CYP3A, or UGT2B7 was assumed to be completely inhibited (i.e., zero) in the presence of their respective inhibitors (Eagling et al., 1998; Sai et al., 2000; Niwa et al., 2005; Khojasteh et al., 2011). This allowed us to estimate CL via the different enzymatic pathways. Then, CL_{int} was estimated using the model-predicted CL, fraction unbound in the incubation ($f_{u,inc}$), and microsomal protein amount as shown in eq. 4. For THC and 11-OH-THC HIM incubations, $f_{u,inc}$ was 0.04 and 0.061 (Patilea-Vrana and Unadkat, 2019) and microsomal protein amount was 0.075 mg and 0.225 mg, respectively.

$$CL_{int} = \frac{CL}{f_{u,inc} * \text{mirosomal protein amount}} \quad (4)$$

Unlike the HIM models, the data from all HFLM experiments were simultaneously fitted to the THC depletion (eq. 5 and 6), 11-OH-THC depletion (eq. 7 and 8), and 1-OH-MDZ formation (eq. 9 and 10) in the absence and presence of AZA. This was done to account for incomplete CYP3A inhibition by AZA in HFLMs, which was estimated as shown in eq. 11. Then, CL_{int} was estimated using eq. 4, but the microsomal protein amount was 0.3 mg for both THC and 11-OH-THC incubations. $F_{u,inc}$ was assumed to be the same as that stated above, as we have previously shown that this value is determined by the BSA rather than the microsomal concentration [0.02 to 0.5 mg/ml (Patilea-Vrana and Unadkat, 2019; Bansal et al., 2022)].

$$\frac{dA_{THC,\ fetal\ liver}}{dt} = -(CL_{CYP3A} + CL_{Other\ CYP}) * C_{THC} \quad (5)$$

$$\frac{dA_{THC+AZA,\ fetal\ liver}}{dt} = -(CL_{CYP3A} * \text{inhibition correction} + CL_{Other\ CYP}) * C_{THC} \quad (6)$$

$$\frac{dA_{11-OH-THC,\ fetal\ liver}}{dt} = -(CL_{CYP3A} + CL_{Other\ CYP}) * C_{11-OH-THC} \quad (7)$$

$$\frac{dA_{11-OH-THC+AZA,\ fetal\ liver}}{dt} = -(CL_{CYP3A} * \text{inhibition correction} + CL_{Other\ CYP}) * C_{11-OH-THC} \quad (8)$$

$$\frac{dA_{1-OH-MDZ,\ fetal\ liver}}{dt} = CL_{CYP3A} * C_{MDZ} \quad (9)$$

$$\frac{dA_{1-OH-MDZ+AZA,\ fetal\ liver}}{dt} = CL_{CYP3A,remaining} * C_{MDZ} \quad (10)$$

$$\text{Fetal liver CYP3A inhibition correction} = \frac{CL_{CYP3A,remaining}}{CL_{CYP3A}} \quad (11)$$

Goodness of model fits was assessed by evaluating the residual plots and % CV of the estimates (which ranged from 14% to 44%, indicating excellent to good confidence in the estimates). Data were weighted using iterative reweighted least squares, where weight = $1/(y_{hat}^2)$, to obtain homoscedasticity in the weighted residual plots.

In Vitro to In Vivo Extrapolation of Kinetic Data. Kinetic parameters estimated from the mathematical models were extrapolated to in vivo whole organ clearance values to ascertain the importance of the estimated in vitro values. Intestinal clearance (CL_{GI}) and fetal liver clearance (CL_{FH}) were calculated using the well-stirred model (eq. 12 and 13, respectively).

$$CL_{GI} = \frac{f_{u,b} * CLint * MPPI * Q_{GI}}{f_{u,b} * CLint * MPPI + Q_{GI}} \quad (12)$$

$$CL_{FH} = \frac{f_{u,b} * CLint * MPPGFL * FLW * Q_{FH}}{f_{u,b} * CLint * MPPGFL * FLW + Q_{FH}} \quad (13)$$

where fraction unbound in blood ($f_{u,b}$) was calculated using the previously reported fraction unbound in plasma ($f_{u,p}$) and blood-to-plasma ratio (B:P) (Giroud et al., 2001; Patilea-Vrana and Unadkat, 2019). The calculated $f_{u,b}$ for THC and 11-OH-THC were 0.016 and 0.019, respectively. Intestinal blood flow (Q_{GI}) is 625 ml/min (Cho et al., 2014), and total microsomal protein per intestine (MPPI) is 3000 mg protein (Hatley et al., 2017). Fetal liver blood flow (Q_{FH}), 56.1 ml/min, was estimated using the average gestational age of the pooled HFLMs as previously described (Zhang et al., 2017). Microsomal protein per gram fetal liver (MPPGFL), 10.1 mg protein/g liver, was calculated using the protein concentrations estimated with the bicinchoninic acid assay and the measured weight of the fetal liver tissue from which the microsomes were isolated. Fetal liver weight (FLW), 8.19 g, was estimated based on gestational age as previously described (Zhang et al., 2017). Fraction that escapes the gut (F_g) and fraction that escapes the fetal liver (F_{fh}) were calculated using eq. 14 and the respective CL parameter.

$$F = 1 - \frac{CL}{Q} \quad (14)$$

Results

THC or 11-OH-THC Depletion Kinetics in Pooled Adult Intestinal Microsomes. At the inhibitor concentrations used, based on published data, we assumed selective and complete inhibition of the respective enzyme (Eagling et al., 1998; Sai et al., 2000; Niwa et al., 2005; Khojasteh et al., 2011). Based on these selective

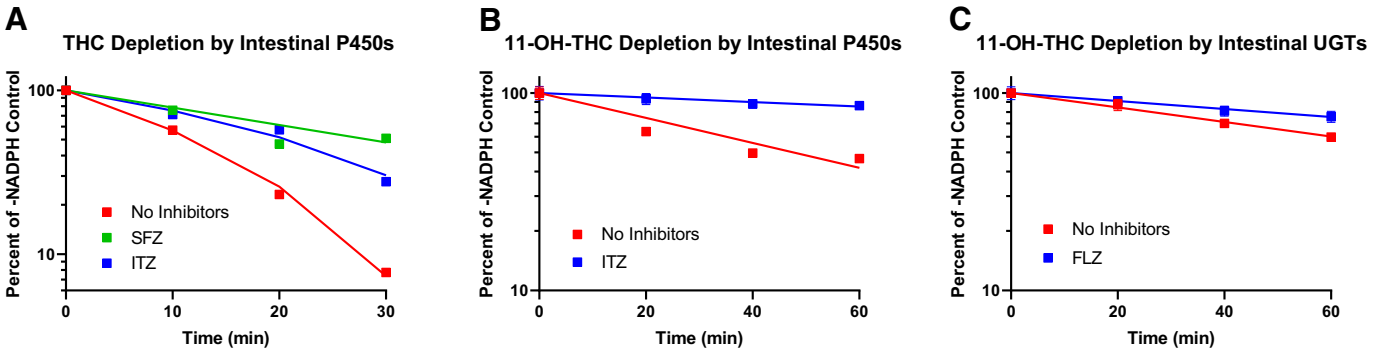

Fig. 1. Depletion of (A) THC (500 nM) and 11-OH-THC (50 nM) by (B) P450 and (C) UGT enzymes in a representative experiment conducted with pooled human adult intestinal microsomes. Lines indicate model fit to the data normalized to data obtained without NADPH. As demonstrated by P450-selective inhibitors, significant metabolism of THC by CYP3A (inhibitor: 2 μM ITZ) and CYP2C9 (inhibitor: 10 μM SFZ) was observed as well as significant metabolism of 11-OH-THC by CYP3A (inhibitor: 2 μM ITZ) and UGT2B7 (inhibitor: 2.5 mM FLZ). Data shown in (B) and (C) are mean ± S.D. of triplicates. Points that do not have error bars have a small S.D. that is within the datapoint. Data shown in (A) are mean of duplicates and therefore do not have error bars. No depletion by CYP1A, CYP2C19, CYP2D6, or FMO enzymes was observed (depletion was not inhibited by inhibitors of these enzymes; data not shown).

TABLE 1

Depletion kinetics of THC and 11-OH-THC in pooled human intestinal microsomes.
Data presented are mean ± S.D. of independent experiments (n = 3–5), each conducted in duplicate or triplicate. CL_{int} was calculated as depletion $CL/f_{u,inc}$.

	THC				11-OH-THC	
	V_{max} (nmol/min/mg)	K_m (nM)	CL_{int}[a] (ml/min/mg)	Fm	CL_{int} (ml/min/mg)	Fm
CYP2C9	1.1 ± 0.38	70 (fixed)	15 ± 5.4	0.89 ± 0.31	NS	NS
CYP3A	NA	NA	2.0 ± 0.86	0.11 ± 0.050	0.26 ± 0.058	0.51 ± 0.11
Total P450	NA	NA	17 ± 6.0	1.0 ± 0.32	0.34 ± 0.080	0.67 ± 0.16
UGT2B7	NA	NA	NS	NS	0.13 ± 0.027	0.25 ± 0.053
Total UGT	NA	NA	NS	NS	0.17 ± 0.024	0.33 ± 0.046

NA, not applicable; NS, not significant.
[a]When CYP2C9 was not saturated.

inhibitors, HIMs significantly metabolized THC via CYP2C9 (SFZ) and CYP3A (ITZ) (Fig. 1A; Table 1) with no involvement by CYP1A, CYP2C19, CYP2D6, FMO, or UGT enzymes (depletion was not inhibited by inhibitors of these enzymes; data not shown). In contrast, HIMs significantly metabolized 11-OH-THC via CYP3A (ITZ) and UGT2B7 (FLZ) (Fig. 1, B and C; Table 1) with no involvement by CYP1A, CYP2C9, CYP2C19, CYP2D6, or FMO enzymes (data not shown). The unsaturated and saturated CL_{GI} of THC were 351 ± 56 ml/min and 83 ± 33 ml/min, respectively, yielding an F_g of 0.44 ± 0.09 and 0.87 ± 0.05, respectively. Also, the CL_{GI} of 11-OH-THC was 29 ± 4.5 ml/min, yielding an F_g of 0.95 ± 0.15.

THC and 11-OH-THC Depletion Kinetics in Pooled Adult Lung Microsomes. HLuMs did not significantly deplete either THC or 11-OH-THC via P450 metabolism (Fig. 2). These microsomes demonstrated CYP1A activity as measured by the NADPH-dependent formation of RES from 7-ER that was inhibitable by ANF (Supplemental Fig. 1).

THC and 11-OH-THC Depletion Kinetics in Placenta Microsomes. HPMs (T1, T2, or term placentae) did not significantly deplete either THC or 11-OH-THC via P450 or UGT metabolism (Fig. 3). As expected, these microsomes demonstrated CYP19 activity as measured by the NADPH-dependent formation of β-estradiol from testosterone (Supplemental Fig. 2).

THC and 11-OH-THC Depletion Kinetics in Pooled Fetal Liver Microsomes. CYP3A was ~67% inhibited by the 5 μM AZA based on inhibition of formation of 1-OH-MDZ from MDZ (Supplemental Fig. 3). Similarly, THC depletion in HFLMs was not completely inhibited by AZA. Therefore, when estimating fraction metabolized (fm) via CYP3A-mediated metabolism of THC and 11-OH-THC, the lack of complete inhibition of CYP3A by AZA was taken into account (see eq. 6, 8, and 11). Based on these and other selective inhibitors, HFLMs were found to significantly metabolize both THC and 11-OH-THC via CYP3A enzymes (Fig. 4; Table 2) with no involvement by CYP2C9 or UGT enzymes (data not shown). Although THC (fm = 0.99) was predominately metabolized by CYP3A, 11-OH-THC (fm = 0.80) was significantly metabolized by other unidentified NADPH-mediated (likely P450) enzyme(s). The fetal liver clearance (CL_{FH}) of THC and 11-OH-THC was 5.7 ± 0.30 ml/min and 3.6 ± 0.21 ml/min, respectively, yielding a fraction that escapes the fetal liver (F_{fh}) of 0.90 and 0.94, respectively.

Discussion

THC and 11-OH-THC were incubated with microsomes at 500 and 50 nM, respectively, to reflect their maximum circulating plasma concentrations (Patilea-Vrana et al., 2019) after inhalation [29.3 mg (Hunault et al., 2008)] and oral administration [90 mg (Lile et al., 2013)] of THC. In the intestine, THC concentrations are likely to be considerably higher than 500 nM, as the maximum fed-state simulated intestinal fluid solubility of THC is 36 μM (Bansal et al., 2020). In the microsomal incubations with THC, formation of 11-OH-THC was not observed. This could be due to either little 11-OH-THC formed during the short incubation period or rapid sequential metabolism of 11-OH-THC or both. Formation of 11-COOH-THC, a metabolite of 11-OH-THC, was also not observed in any of the THC or 11-OH-THC P450 microsomal incubations, possibly due to limited experimental timeframe or the lower abundance of CYP2C9 in intestinal microsomes or both.

In the absence of CYP2C9 inhibition, the depletion of THC in HIMs was not log-linear since the slope of the depletion curve increased with time (Fig. 1A). This was not the case in the presence of CYP2C9

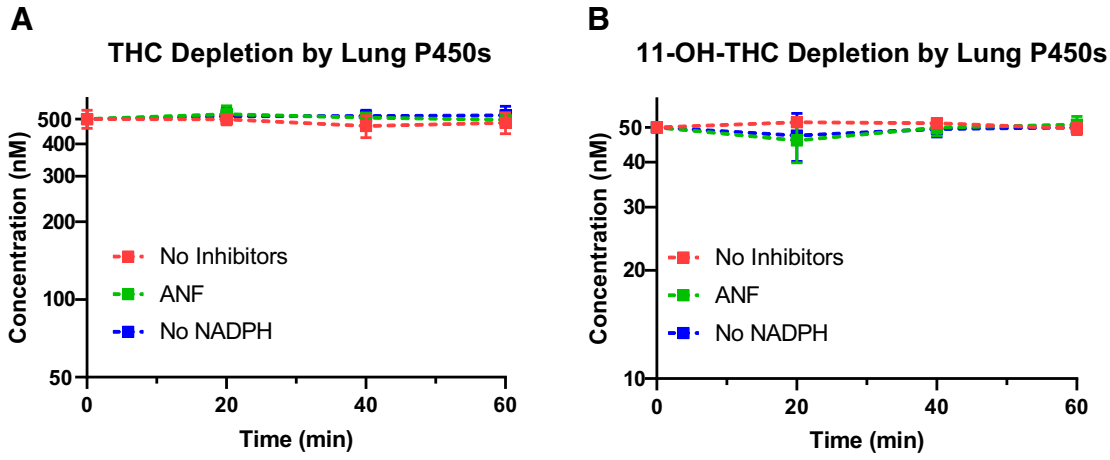

Fig. 2. Depletion of (A) THC (500 nM) or (B) 11-OH-THC (50 nM) by P450 enzymes in pooled human adult lung microsomes (cigarette smokers). No significant depletion of THC or 11-OH-THC was observed in lung microsomes. Data shown are mean ± S.D. of independent experiments (n = 3), each conducted in duplicate. ANF (3 μM): CYP1A inhibitor.

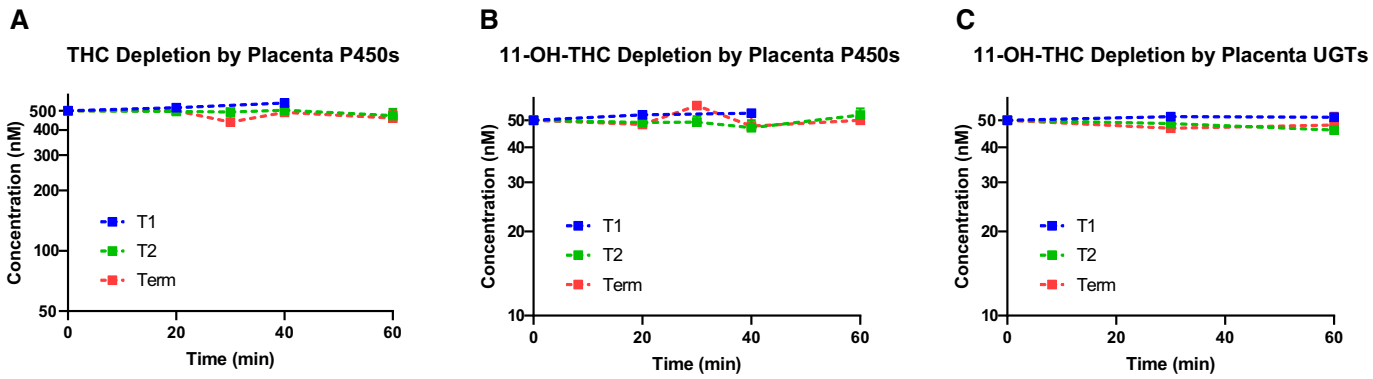

Fig. 3. Depletion of (A) THC (500 nM) or 11-OH-THC (50 nM) by (B) P450 or (C) UGT enzymes in human T1, T2, and term placental microsomes. No significant depletion of THC or 11-OH-THC was observed in the placental microsomes. Data shown are mean ± S.D. (where applicable) of one to four independent experiments, each conducted in singlicate or duplicate. Microsomes were isolated from T1 placentae (blue, no S.D. shown) at gestational ages 79 and 96 days; T2 (green, no S.D. shown for 11-OH-THC UGT depletion) at gestational ages 134, 135, and 137 days; and Term (red, two placentae for P450 and three for UGT depletion).

inhibition. These observations are typical of saturable metabolism and consistent with our previous data in human liver microsomes (Patilea-Vrana and Unadkat, 2019), where saturation of CYP2C9 was observed (THC K_m of 70 nM, K_m unbound of 2.91 nM). Consistent with these data, when THC was incubated at 50 nM, depletion in HIMs was found to be log-linear (data not shown). However, further experiments at this concentration were not conducted due to lack of analytical sensitivity, which limited our ability to determine THC depletion with confidence. CYP2C9 is the second most abundant P450 enzyme, after CYP3A, in the human intestine, and it has previously been shown to metabolize drugs in HIMs (Galetin and Houston, 2006; Paine et al., 2006; Drozdzik et al., 2018). Therefore, saturable kinetics of CYP2C9 was built into the kinetic model used to fit to the THC depletion data in HIMs. When CYP2C9 is partially saturated (e.g., at 10 minutes in Fig. 1A), the estimated fm of CYP2C9 is 0.58 ± 0.09 versus 0.89 ± 0.31 when unsaturated and the corresponding estimated fm of CYP3A is 0.60 ± 0.22 versus 0.11 ± 0.05.

The slope of 11-OH-THC depletion appears to decrease with time in both the intestinal and fetal liver microsomes in each individual experiment as well as the mean data (Figs. 1B and 4B). The basis for these observations is unknown but could be due to lower enzyme activity over time, either from product inhibition or enzyme instability in the incubations. The latter is unlikely, as this has not been observed for other CYP3A substrates (Davies et al., 2020). UGTs (fm = 0.33) also depleted 11-OH-THC in HIMs. We have previously shown that recombinant UGT2B7 and UGT1A9 metabolize 11-OH-THC (Patilea-Vrana et al., 2019). Here we observed no significant inhibition of 11-OH-THC depletion by NFA, a semiselective UGT1A9 inhibitor (data not shown). Therefore, we concluded that inhibition of 11-OH-THC metabolism by FLZ (a semiselective UGT2B7 inhibitor) was entirely due to UGT2B7, an enzyme found in the human intestines (Wu et al., 2011).

Although there was significant metabolism observed in the HIMs, the whole organ CL of THC and 11-OH-THC was approximately 1/4 and 1/50 of their respective hepatic CL [THC: 1500 ml/min; 11-OH-THC: 1350 ml/min (Patilea-Vrana and Unadkat, 2019)]. This is consistent with the lower abundance of CYP2C9 and CYP3A in the intestine (0.0084 and 0.059 nmol/mg protein, respectively) versus the liver (0.060 and 0.096 nmol/mg protein, respectively) (Shimada et al., 1994; Paine et al., 2006) and a lower abundance of UGTs (Drozdzik et al., 2018). Nevertheless, intestinal metabolism could still contribute to the low oral bioavailability of THC by first-pass gut metabolism. Indeed, the estimated F_g of THC (from observed intravenous and oral administration data), assuming fraction absorbed (F_a) = 1, is 0.17 (Ohlsson et al., 1980, 1982). Assuming a common 20-mg THC oral dose and an average intestinal volume of 250 ml, the THC concentration in the gut would be ~250 μM, which exceeds the maximum solubility in fed-state

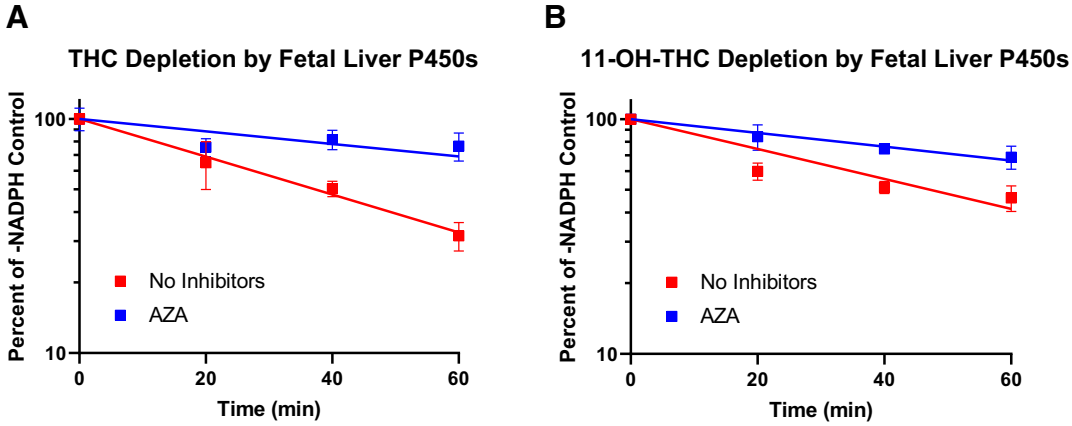

Fig. 4. Depletion of (A) THC (500 nM) or (B) 11-OH-THC (50 nM) by P450 enzymes in pooled human fetal liver microsomes. Lines indicate model fit to the data normalized to those obtained without NADPH. Significant metabolism of THC and 11-OH-THC by CYP3A was observed in the fetal liver microsomes, as evidenced by inhibition by AZA (5 μM). Data shown are mean ± S.D. of three independent experiments, each conducted in duplicate. Points that do not have error bars have a small S.D. that is within the datapoint. No depletion by CYP2C9 or UGT enzymes was observed (depletion was not inhibited by inhibitors of these enzymes; data not shown).

TABLE 2

Depletion kinetics of THC and 11-OH-THC in pooled human fetal liver microsomes.
Data presented are mean ± S.D. of four independent experiments. CL_{int} was calculated as depletion $CL/f_{u,inc}$.

	THC		11-OH-THC	
	CL_{int} (ml/min/mg)	Fm	CL_{int} (ml/min/mg)	Fm
CYP3A	4.6 ± 0.17	0.99 ± 0.06	1.9 ± 0.11	0.80 ± 0.06
Total P450	4.7 ± 0.22	1	2.4 ± 0.13	1

simulated intestinal fluid (~36 μM (Bansal et al., 2020)). The latter would far exceed the CYP2C9 K_m (70 nM) and saturate the enzyme, resulting in a predicted F_g of THC of 0.87 ± 0.05 due to CYP3A first-pass effect metabolism. This discrepancy between in vivo and in vitro estimate of F_g is likely due to the F_a of THC being <1 (estimated from these data as ~0.2). We speculate that after oral administration of THC, THC is incompletely absorbed and experiences limited first-pass metabolism in the intestine, predominately by CYP3A. Thus, we predict mostly CYP2C9-based DDI at the hepatic level (first-pass and systemic) after oral administration of THC. Indeed, CYP2C9 genetic polymorphism with homozygote *3 alleles increases oral THC plasma exposure [area under the curve (AUC)] (Sachse-Seeboth et al., 2009).

Of the many recombinant enzymes tested, CYP1A1 turnover of THC and 11-OH-THC was the highest per pmol of the P450 enzyme (Patilea-Vrana et al., 2019). Because human lungs (and placentae) highly express CYP1A1 enzyme (Hukkanen et al., 2001; Suter et al., 2010), we speculated that THC would be metabolized in microsomes from these organs. However, no significant THC depletion was observed in lung (from cigarette smokers) and placenta microsomes, despite the fact that these microsomes had functional P450 activity. Although CYP1A is expressed and active in human lung tissue, its role in in vivo lung CYP1A metabolism has never been confirmed (Hukkanen et al., 2001; Enlo-Scott et al., 2021). Therefore, we conclude that inhaled THC will not undergo first-pass CYP1A metabolism in the lungs.

Data in fetal-catheterized rhesus macaques show that fetal THC plasma AUC is 0.37 of the corresponding maternal plasma AUC (Bailey et al., 1987). Theoretically, assuming that the plasma protein binding of THC is the same or similar in the maternal and fetal compartment, and if THC is not effluxed by the placental transporters (P-glycoprotein and breast cancer resistance protein) or metabolized in the placenta or fetal liver, the fetal-maternal unbound plasma AUC ratio (K_p) should be unity (Zhang et al., 2017). Thus, a ratio of 0.37 suggests possible placental or fetal liver metabolism or placental efflux of the drug. However, data from our laboratory have shown that THC is not a substrate of human P-glycoprotein or breast cancer resistance protein (Chen et al., 2021). Therefore, we speculated that THC is metabolized by either the placenta or the fetal liver or both.

Placentae from women who smoke cigarettes demonstrate increased CYP1A1 enzyme activity and mRNA expression (Smith et al., 2001; Suter et al., 2010). CYP19 is also highly expressed in the placenta (Hakkola et al., 1998). Nevertheless, consistent with our HLuM data and no turnover by recombinant CYP19 (Patilea-Vrana et al., 2019), we found no depletion of THC or 11-OH-THC in human placentae at any gestational age. In contrast, significant CYP3A-mediated depletion of THC and 11-OH-THC was observed in pooled HFLMs. The previously mentioned decreasing slope of 11-OH-THC depletion over time is what likely caused the lower estimated CYP3A fm of 0.80. If the rate of depletion throughout the run was consistent with the elimination rate within the first 20 minutes (Fig. 4B), the fm of CYP3A would have been closer to 0.95. Due to the smaller fetal liver size (compared with maternal liver), we estimated that the fetal hepatic CL of THC and 11-OH-THC was approximately 1/290 and 1/230 of their respective adult hepatic CL, contributing very little to the overall maternal THC CL. Nevertheless, such metabolism could explain a fetal THC K_p of less than unity (observed in macaques), provided that the fetal THC CL is significant relative to its transplacental CL (all unbound) (Zhang et al., 2017). Therefore, it is imperative to determine the transplacental CL of THC. Such studies are ongoing in our laboratory using the perfused human placenta.

In conclusion, we quantified the enzyme kinetics of THC and 11-OH-THC in extrahepatic tissues (intestine, fetal liver, lung, and placenta). In the intestine, THC (at subsaturating concentrations) was significantly metabolized by CYP2C9 and CYP3A, whereas 11-OH-THC was significantly metabolized by CYP3A and UGT2B7. In the fetal liver, both compounds were significantly metabolized by CYP3A. There was no significant metabolism of either cannabinoid in the human lung or placenta. Populating a THC/11-OH-THC PBPK model with the enzyme kinetics estimated here is necessary to predict THC and 11-OH-THC disposition in healthy adults. Once such a PBPK model is verified in healthy adults, it can be used to predict the disposition of these drugs in special populations where enzyme abundances and activities are altered by genetic polymorphism [e.g., CYP2C9 (Mamiya et al., 1998)] or physiologic changes (e.g., hepatic impairment and pregnancy). The kinetic parameters calculated here and from our ongoing perfused human placenta studies will be used to populate our maternal-fetal–PBPK model to predict maternal-fetal exposure to THC and 11-OH-THC PK after both oral and inhalational cannabis use. Such predictions will help assess risk to the fetus after maternal cannabis consumption.

Acknowledgments

We thank the Birth Defects Research Laboratory (Seattle, WA) for acquiring human placentae and human fetal liver tissue.

Authorship Contributions

Participated in research design: Kumar, Patilea-Vrana, Unadkat.
Conducted experiments: Kumar, Patilea-Vrana, Anoshchenko.
Performed data analysis: Kumar.
Wrote or contributed to the writing of the manuscript: Kumar, Patilea-Vrana, Anoshchenko, Unadkat.

References

Amin MR and Ali DW (2019) Pharmacology of medical cannabis. *Adv Exp Med Biol* **1162**: 151–165.
Anoshchenko O, Prasad B, Neradugomma NK, Wang J, Mao Q, and Unadkat JD (2020) Gestational age-dependent abundance of human placental transporters as determined by quantitative targeted proteomics. *Drug Metab Dispos* **48**:735–741.
Bailey JR, Cunny HC, Paule MG, and Slikker Jr W (1987) Fetal disposition of delta 9-tetrahydrocannabinol (THC) during late pregnancy in the rhesus monkey. *Toxicol Appl Pharmacol* **90**:315–321.
Bansal S, Maharao N, Paine MF, and Unadkat JD (2020) Predicting the potential for cannabinoids to precipitate pharmacokinetic drug interactions via reversible inhibition or inactivation of major cytochromes P450. *Drug Metab Dispos* **48**:1008–1017.
Bansal S, Paine MF, and Unadkat JD (2022) Comprehensive predictions of cytochrome P450 (CYP)-mediated in vivo cannabinoid-drug interactions based on reversible and time-dependent CYP inhibition in human liver microsomes. *Drug Metab Dispos* **50**:351–360.

Chen X, Unadkat JD, and Mao Q (2021) Tetrahydrocannabinol and its major metabolites are not (or are poor) substrates or inhibitors of human P-glycoprotein [ATP-binding cassette (ABC) B1] and breast cancer resistance protein (ABCG2). *Drug Metab Dispos* **49**:910–918.

Cho HJ, Kim JE, Kim DD, and Yoon IS (2014) In vitro-in vivo extrapolation (IVIVE) for predicting human intestinal absorption and first-pass elimination of drugs: principles and applications. *Drug Dev Ind Pharm* **40**:989–998.

Davies M, Peramuhendige P, King L, Golding M, Kotian A, Penney M, Shah S, and Manevski N (2020) Evaluation of in vitro models for assessment of human intestinal metabolism in drug discovery. *Drug Metab Dispos* **48**:1169–1182.

Day NL, Richardson GA, Goldschmidt L, Robles N, Taylor PM, Stoffer DS, Cornelius MD, and Geva D (1994) Effect of prenatal marijuana exposure on the cognitive development of offspring at age three. *Neurotoxicol Teratol* **16**:169–175.

Drozdzik M, Busch D, Lapczuk J, Müller J, Ostrowski M, Kurzawski M, and Oswald S (2018) Protein abundance of clinically relevant drug-metabolizing enzymes in the human liver and intestine: a comparative analysis in paired tissue specimens. *Clin Pharmacol Ther* **104**:515–524.

Eagling VA, Tjia JF, and Back DJ (1998) Differential selectivity of cytochrome P450 inhibitors against probe substrates in human and rat liver microsomes. *Br J Clin Pharmacol* **45**:107–114.

Enlo-Scott Z, Bäckström E, Mudway I, and Forbes B (2021) Drug metabolism in the lungs: opportunities for optimising inhaled medicines. *Expert Opin Drug Metab Toxicol* **17**:611–625.

Galetin A and Houston JB (2006) Intestinal and hepatic metabolic activity of five cytochrome P450 enzymes: impact on prediction of first-pass metabolism. *J Pharmacol Exp Ther* **318**:1220–1229.

Giroud C, Ménétrey A, Augsburger M, Buclin T, Sanchez-Mazas P, and Mangin P (2001) Delta(9)-THC, 11-OH-Delta(9)-THC and Delta(9)-THCCOOH plasma or serum to whole blood concentrations distribution ratios in blood samples taken from living and dead people. *Forensic Sci Int* **123**:159–164.

Goldschmidt L, Day NL, and Richardson GA (2000) Effects of prenatal marijuana exposure on child behavior problems at age 10. *Neurotoxicol Teratol* **22**:325–336.

Goldschmidt L, Richardson GA, Willford J, and Day NL (2008) Prenatal marijuana exposure and intelligence test performance at age 6. *J Am Acad Child Adolesc Psychiatry* **47**:254–263.

Goldschmidt L, Richardson GA, Willford JA, Severtson SG, and Day NL (2012) School achievement in 14-year-old youths prenatally exposed to marijuana. *Neurotoxicol Teratol* **34**:161–167.

Grotenhermen F (2003) Pharmacokinetics and pharmacodynamics of cannabinoids. *Clin Pharmacokinet* **42**:327–360.

Hakkola J, Pelkonen O, Pasanen M, and Raunio H (1998) Xenobiotic-metabolizing cytochrome P450 enzymes in the human feto-placental unit: role in intrauterine toxicity. *Crit Rev Toxicol* **28**:35–72.

Hatley OJ, Jones CR, Galetin A, and Rostami-Hodjegan A (2017) Quantifying gut wall metabolism: methodology matters. *Biopharm Drug Dispos* **38**:155–160.

Hukkanen J, Pelkonen O, and Raunio H (2001) Expression of xenobiotic-metabolizing enzymes in human pulmonary tissue: possible role in susceptibility for ILD. *Eur Respir J Suppl* **32**:122s–126s.

Hunault CC, Mensinga TT, de Vries I, Kelholt-Dijkman HH, Hoek J, Kruidenier M, Leenders ME, and Meulenbelt J (2008) Delta-9-tetrahydrocannabinol (THC) serum concentrations and pharmacological effects in males after smoking a combination of tobacco and cannabis containing up to 69 mg THC. *Psychopharmacology (Berl)* **201**:171–181.

Khojasteh SC, Prabhu S, Kenny JR, Halladay JS, and Lu AY (2011) Chemical inhibitors of cytochrome P450 isoforms in human liver microsomes: a re-evaluation of P450 isoform selectivity. *Eur J Drug Metab Pharmacokinet* **36**:1–16.

Leeder JS, Gaedigk R, Marcucci KA, Gaedigk A, Vyhlidal CA, Schindel BP, and Pearce RE (2005) Variability of CYP3A7 expression in human fetal liver. *J Pharmacol Exp Ther* **314**:626–635.

Lile JA, Kelly TH, Charnigo RJ, Stinchcomb AL, and Hays LR (2013) Pharmacokinetic and pharmacodynamic profile of supratherapeutic oral doses of Δ(9) -THC in cannabis users. *J Clin Pharmacol* **53**:680–690.

Lucas CJ, Galettis P, and Schneider J (2018) The pharmacokinetics and the pharmacodynamics of cannabinoids. *Br J Clin Pharmacol* **84**:2477–2482.

Mamiya K, Ieiri I, Shimamoto J, Yukawa E, Imai J, Ninomiya H, Yamada H, Otsubo K, Higuchi S, and Tashiro N (1998) The effects of genetic polymorphisms of CYP2C9 and CYP2C19 on phenytoin metabolism in Japanese adult patients with epilepsy: studies in stereoselective hydroxylation and population pharmacokinetics. *Epilepsia* **39**:1317–1323.

Niwa T, Shiraga T, and Takagi A (2005) Effect of antifungal drugs on cytochrome P450 (CYP) 2C9, CYP2C19, and CYP3A4 activities in human liver microsomes. *Biol Pharm Bull* **28**:1805–1808.

Ohlsson A, Lindgren JE, Wahlen A, Agurell S, Hollister LE, and Gillespie HK (1980) Plasma delta-9 tetrahydrocannabinol concentrations and clinical effects after oral and intravenous administration and smoking. *Clin Pharmacol Ther* **28**:409–416.

Ohlsson A, Lindgren JE, Wahlén A, Agurell S, Hollister LE, and Gillespie HK (1982) Single dose kinetics of deuterium labelled delta 1-tetrahydrocannabinol in heavy and light cannabis users. *Biomed Mass Spectrom* **9**:6–10.

Paine MF, Hart HL, Ludington SS, Haining RL, Rettie AE, and Zeldin DC (2006) The human intestinal cytochrome P450 "pie". *Drug Metab Dispos* **34**:880–886.

Patilea-Vrana GI, Anoshchenko O, and Unadkat JD (2019) Hepatic enzymes relevant to the disposition of (-)-Δ^9-tetrahydrocannabinol (THC) and its psychoactive metabolite, 11-OH-THC. *Drug Metab Dispos* **47**:249–256.

Patilea-Vrana GI and Unadkat JD (2019) Quantifying hepatic enzyme kinetics of (-)-Δ^9-tetrahydrocannabinol (THC) and its psychoactive metabolite, 11-OH-THC, through in vitro modeling. *Drug Metab Dispos* **47**:743–752.

Paul SE, Hatoum AS, Fine JD, Johnson EC, Hansen I, Karcher NR, Moreau AL, Bondy E, Qu Y, Carter EB, et al. (2021) Associations between prenatal cannabis exposure and childhood outcomes: results from the ABCD Study. *JAMA Psychiatry.* **78**:64–76.

Sachse-Seeboth C, Pfeil J, Sehrt D, Meineke I, Tzvetkov M, Bruns E, Poser W, Vormfelde SV, and Brockmöller J (2009) Interindividual variation in the pharmacokinetics of Delta9-tetrahydrocannabinol as related to genetic polymorphisms in CYP2C9. *Clin Pharmacol Ther* **85**:273–276.

Sai Y, Dai R, Yang TJ, Krausz KW, Gonzalez FJ, Gelboin HV, and Shou M (2000) Assessment of specificity of eight chemical inhibitors using cDNA-expressed cytochromes P450. *Xenobiotica* **30**:327–343.

PAMHSA (2021) Key substance use and mental health indicators in the United States: results from the 2020 National Survey on Drug Use and Health (HHS Publication No. PEP21-07-01-003, NSDUH Series H-56). Center for Behavioral Health Statistics and Quality, Substance Abuse and Mental Health Services Administration, Rockville, MD.

Shimada T, Yamazaki H, Mimura M, Inui Y, and Guengerich FP (1994) Interindividual variations in human liver cytochrome P-450 enzymes involved in the oxidation of drugs, carcinogens and toxic chemicals: studies with liver microsomes of 30 Japanese and 30 Caucasians. *J Pharmacol Exp Ther* **270**:414–423.

Smith GB, Harper PA, Wong JM, Lam MS, Reid KR, Petsikas D, and Massey TE (2001) Human lung microsomal cytochrome P4501A1 (CYP1A1) activities: impact of smoking status and CYP1A1, aryl hydrocarbon receptor, and glutathione S-transferase M1 genetic polymorphisms. *Cancer Epidemiol Biomarkers Prev* **10**:839–853.

Suter M, Abramovici A, Showalter L, Hu M, Shope CD, Varner M, and Aagaard-Tillery K (2010) In utero tobacco exposure epigenetically modifies placental CYP1A1 expression. *Metabolism* **59**:1481–1490.

Wu B, Kulkarni K, Basu S, Zhang S, and Hu M (2011) First-pass metabolism via UDP-glucuronosyltransferase: a barrier to oral bioavailability of phenolics. *J Pharm Sci* **100**: 3655–3681.

Zhang Z, Imperial MZ, Patilea-Vrana GI, Wedagedera J, Gaohua L, and Unadkat JD (2017) Development of a novel maternal-fetal physiologically based pharmacokinetic model I: insights into factors that determine fetal drug exposure through simulations and sensitivity analyses. *Drug Metab Dispos* **45**:920–938.

Address correspondence to: Dr. Jashvant D. Unadkat, University of Washington, Department of Pharmaceutics, PO Box 357610, Seattle, WA 98195. E-mail: jash@u.washington.edu

Drug Metabolism and Disposition: DMD-AR-2022-000868

Characterizing and Quantifying Extrahepatic Metabolism of (-)-Δ^9-Tetrahydrocannabinol (THC) and Its Psychoactive Metabolite, 11-OH-THC

Aditya R. Kumar, Gabriela I. Patilea-Vrana, Olena Anoshchenko, Jashvant D. Unadkat

Department of Pharmaceutics, University of Washington, Seattle Washington (A.R.K., G.I.P., O.A., J.D.U.)

Supplemental Table 1: Demographics of the Human Placentae

Subject ID	Gestational Age (days)	Trimester	Fetal Sex (M/F)	Maternal Age (years)	Maternal Ethnicity
PL040	96	T1	M	26	White
PL987	79	T1	Unknown	18	Hispanic
PL037	135	T2	F	33	White
PL041	137	T2	F	Unknown	Unknown
PL946	134	T2	F	21	White/Hispanic
PL1	---	Term	Unknown	Unknown	Unknown
PL5	----	Term	Unknown	Unknown	Unknown
PL6	---	Term	Unknown	Unknown	Unknown

T1: 1 – 97 days; T2: 98 – 195 days; Term: at delivery

Supplemental Table 2: Demographics of Human Fetal Livers

Subject ID	Gestational Age (days)	Trimester	Fetal Sex (M/F)	Maternal Age (years)	Maternal Ethnicity	Alcohol Use (Y/N)
H26872	113	T2	F	32	Black	N
H27078	119	T2	M	26	White	N
H27164	127	T2	F	22	White	N
H27257	113	T2	Unknown	22	Mixed	Y
H27360	115	T2	M	Unknown	Unknown	Unknown
H27723	125	T2	F	Unknown	Unknown	Unknown

T2: 98 – 195 days

Supplemental Table 3: LC-MS/MS parameters of drug quantification

A. LC gradient program

Time (min)	Flow Rate (mL/min)	A (water with 0.1% formic acid, %)	B (acetonitrile with 0.1% formic acid, %)
0	0.3	90	10
0.5	0.3	90	10
2	0.3	5	95
4	0.3	5	95
4.1	0.3	90	10
4.5	0.3	90	10

B. MS/MS parameters

Compound	Parent Ion (m/z)	Product Ion (m/z)	Declustering Potential (V)	Collision Energy (V)	Collision Cell Exit Potential (V)
THC	315.2	193.3	100	33	10
d3-THC	318.3	196.3	100	33	10
11-OH-THC	331.4	193.3	150	35	15
d3-11-OH-THC	334.4	196.3	150	35	15
COOH-THC	345.3	327.3	150	23	15
d3-COOH-THC	348.3	330.3	150	23	15
1-OH-MDZ	342.1	324.0	170	30	20
d4-OH-MDZ	346.1	328.1	170	30	20

RES	214.0	186.0	120	40	10
TOL	271.3	155.0	60	30	6
β-estradiol	255.0	159.1	80	30	9
d4-β-estradiol	259.0	161.0	80	40	9

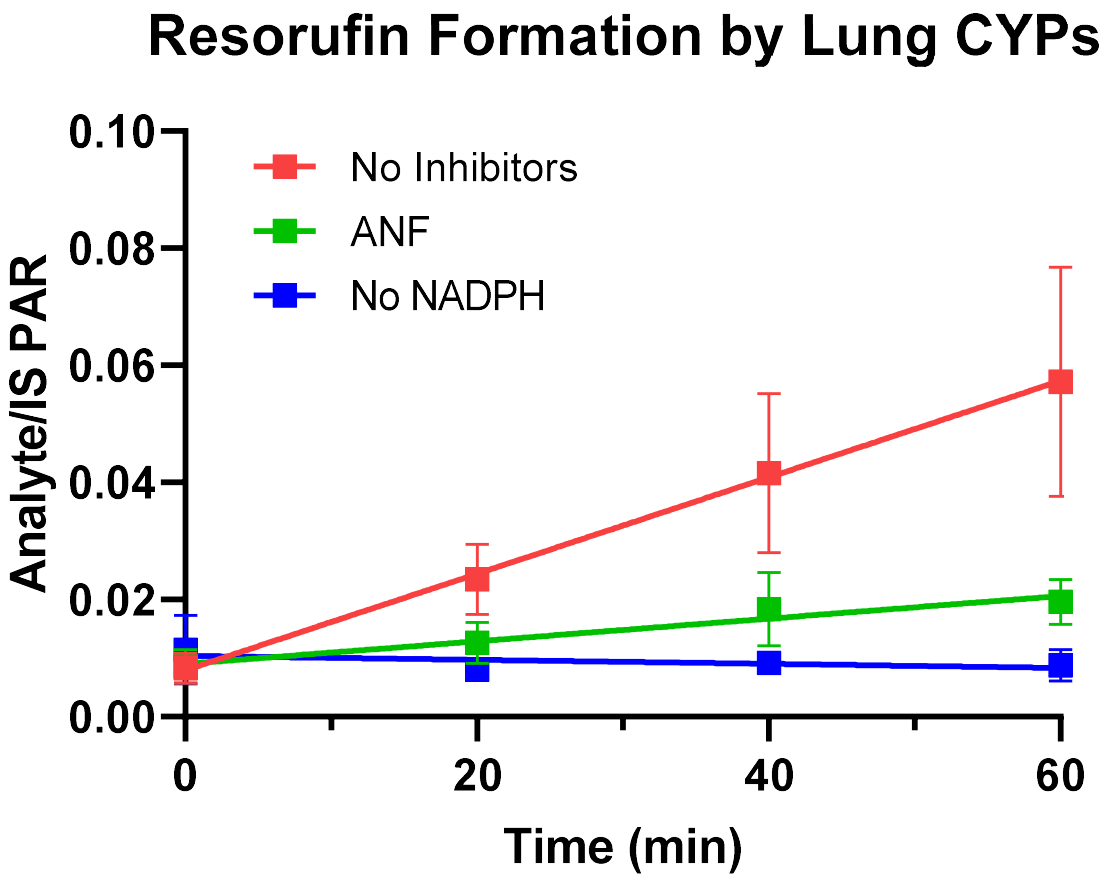

Supplemental Figure 1: Formation of resorufin from 7-ethoxyresorufin in pooled human adult lung microsomes (cigarette smokers). Lines indicate linear regression fit to the data. Formation of resorufin was inhibited by the CYP1A inhibitor, ANF (3 μM), indicating that the HLuM demonstrate CYP1A activity. Data shown (peak area ratio of the analyte to the internal standard) are mean of 2 independent experiments, each conducted in duplicate.

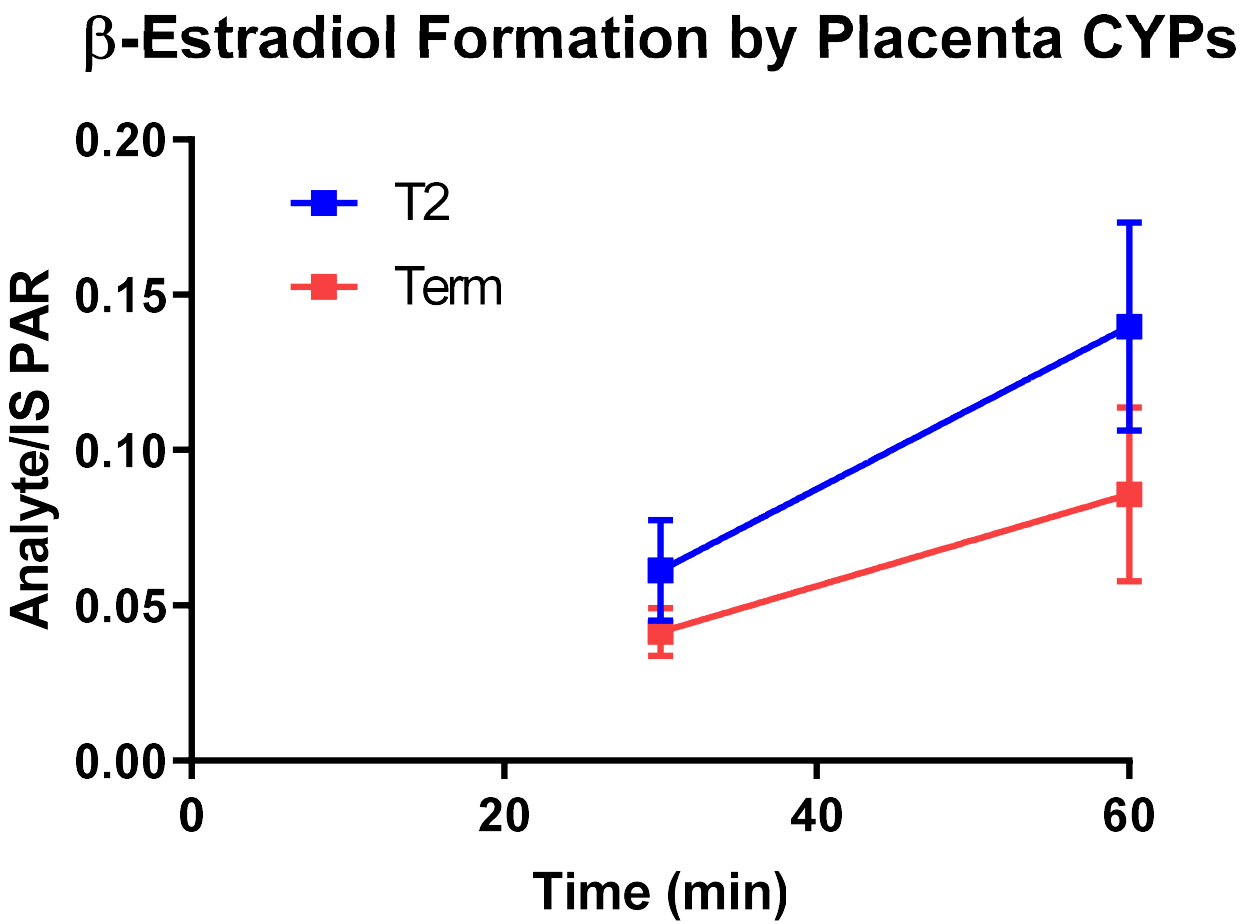

Supplemental Figure 2: Formation of β-Estradiol (CYP19) from testosterone in human T2 and term placental microsomes. Lines indicate linear regression fit to the data. Data shown (as peak area ratio of the analyte to the internal standard) are mean of triplicate incubations from one experiment. Microsomes were isolated from T2 placentae (blue; gestational ages 134 and 135 days), and Term (red, one donor).

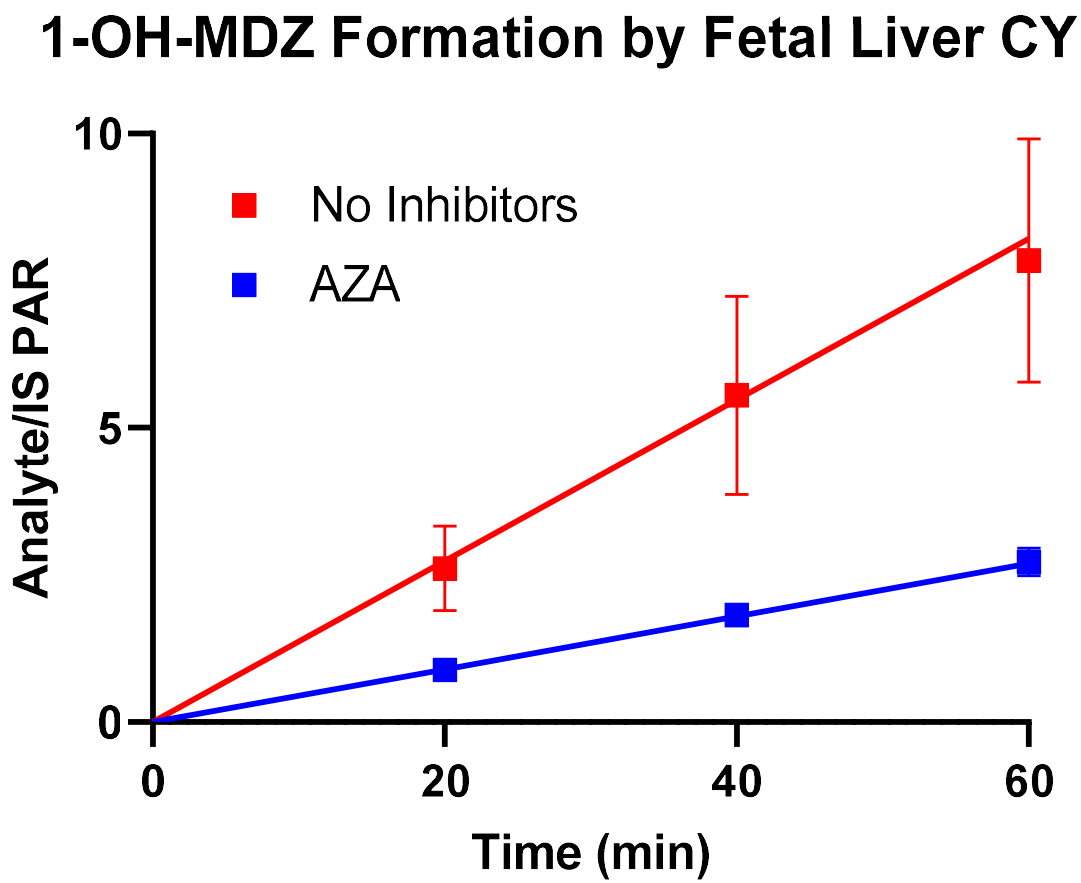

Supplemental Figure 3: Formation of 1-OH-MDZ from MDZ in pooled human fetal liver microsomes. Lines indicate model fit to the data normalized to those obtained without NADPH. Formation of 1-OH-MDZ was inhibited by the CYP3A inhibitor, AZA (5 μM). Data shown (as peak area ratio of the analyte to the internal standard) are mean ± SD of 3 independent experiments, each conducted in duplicate.